

## SUPPORTING INFORMATION:

# A Nanoscale-Modified LaMer Model for Particle Synthesis from Inorganic Tin-Platinum Complexes

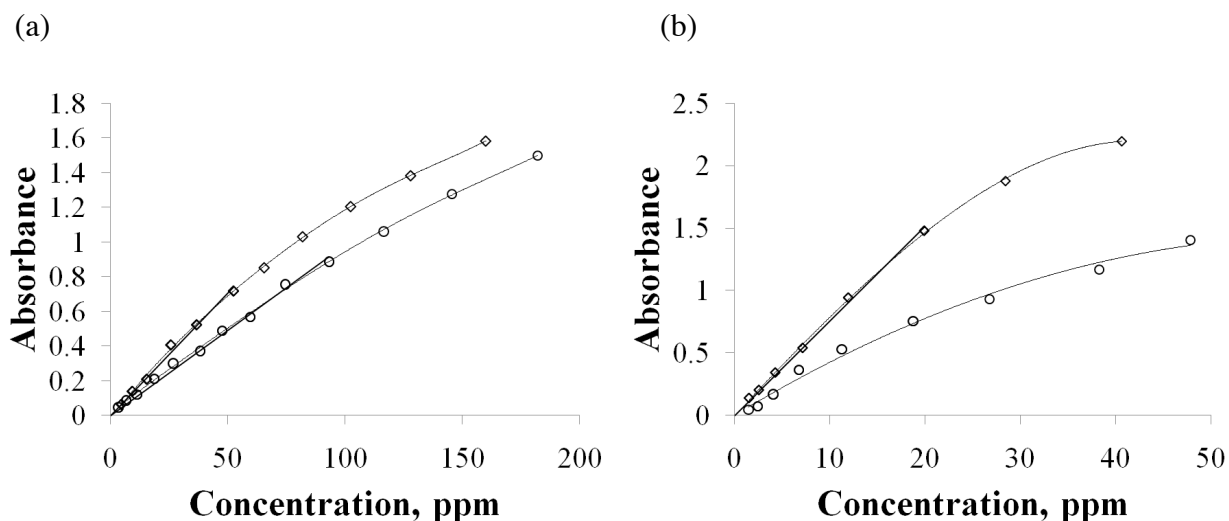
*Samuel St. John, Naiping Hu, Dale W. Schaefer, Anastasios P. Angelopoulos\**

Department of Chemical Engineering, School of Energy, Environmental, and Biological &  
Medical Engineering, University of Cincinnati, Cincinnati, OH 45221

### SI 1. EXPERIMENTAL METHODS

**SI 1.1 UV-vis Spectroscopy Apparatus and Standard Curves.** UV-vis spectroscopy was used to determine the Sn-Pt complex stoichiometry and to follow the kinetics of Pt reduction during nanoparticle synthesis. Absorbance measurements were made with an Ocean Optics model HR2000+CG-UV-NIR photodiode array spectrophotometer with a DH-2000-BAL deuterium/halogen UV-vis-near-infrared (NIR) light source. Measurements were made from 200 to 1000 nm with 3.5 s temporal averaging. Samples were maintained under nitrogen atmosphere except briefly when measurements were taken in 1.000 cm silica quartz cells (Spectrosil Quartz, Starna Cells, Inc.) for mole ratio method measurements and disposable 1.000 cm polystyrene cuvettes (polystyrene, Plastibrand) for kinetics analysis. Mixing of reagents was done by nitrogen bubbling and transfer done with precision, positive-pressure liquid pipettes.

**SI 1.2 Standard Curves used in UV-vis Spectroscopy.** Several standardization curves were developed to ensure that diluted quantities of the Sn(II), Sn(IV), Pt(II), and Pt(IV) behaved according to Beer's Law in the concentration ranges of interest. Concentrated solutions were prepared according to the procedure given in the experimental section of the main document. A 7.5  $\mu\text{L}$  sample was then pipetted into 1.5 mL of 7.5 M, nitrogen saturated, 5°C hydrochloric acid. Once the measurement was taken, a portion of the original sample was then diluted with 7.5 M, nitrogen-saturated, room-temperature hydrochloric acid. All concentrations investigated were prepared by serial dilution in this way. Based on the calibration curves, the optimum concentration of Pt in solution is from 5 to 20 ppm. Fortunately, the optimum concentration of Sn in solution spanned the range needed for the desired mole ratios for the investigation described in the next section. The calibration curves in the concentration regions of interest are in SI Figure 1(a,b). Sn(IV) is not photoactive in the region of interest for both the mole ratio and kinetics investigation.



SI Figure 1: Absorbance versus wavelength of (a) Sn(II) at 260 nm, *circles*, and Sn(IV) at 242 nm, *diamonds*, in 7.5 M, nitrogen-saturated hydrochloric acid; (b) Pt(II) at 227 nm, *circles*, and

Pt(IV) at 261 nm, *diamonds*, in 7.5 M, nitrogen-saturated hydrochloric acid. The linear regression segments indicate the region of interest for the mole ratio analysis.

**SI 1.3 Determining Sn-Pt Complex Stoichiometry.** We determined the Sn-Pt complex stoichiometry using the mole ratio method. In this method, we combined Sn and Pt at different molar ratios and measured the UV-vis absorbance at three concentrations to determine the extinction coefficient of the Sn-Pt complex that formed. The extinction coefficient is a fundamental material property of the Sn-Pt complex. Changes in the extinction coefficient as a function of the molar ratio of Sn to Pt reflect a change in the structure of the Sn-Pt complex. A complete mathematical treatment of the mole ratio is given by Meyer for Sn/Pt systems.<sup>1-3</sup>

Small amounts of Pt(II) or Pt(IV) solution described above were mixed with Sn(II) solution under nitrogen bubbling to give a total combined volume of 0.5 mL. Comparison of the extinction coefficient spectrum will let us determine if different complexes form with Pt(II) and Pt(IV) or if Pt(IV) is first reduced. We can thus investigate the first reduction step for nanoparticle synthesis.

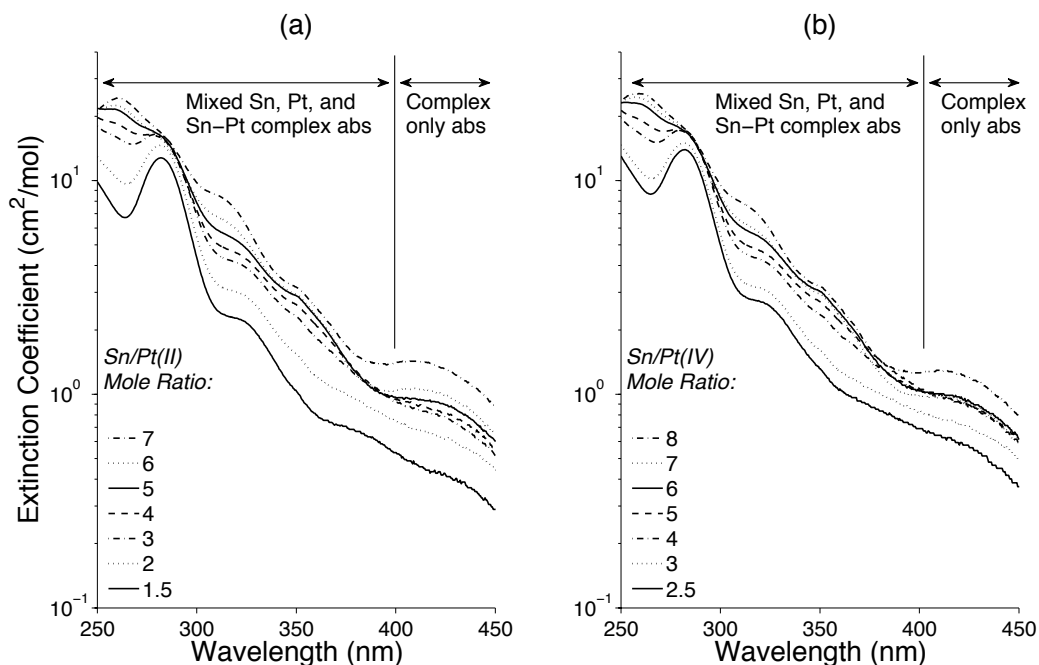
When Pt(II) or Pt(IV) solutions were mixed with Sn(II), the solutions turned a deep red that intensified over time but stabilized at ambient conditions and nitrogen bubbling after 15 minutes. The quantity of the tin solution was varied to investigate different Sn/Pt mole ratios at constant Pt concentration. Constant solution volume was maintained with make-up quantities of 7.5 M, nitrogen-saturated, 5°C hydrochloric acid. Mole ratios were varied from 1.5:1 to 7:1 and their absorbencies were measured by pipetting 15, 10, and 5  $\mu\text{L}$  into 1.5 mL of 7.5 M, nitrogen-saturated, hydrochloric acid solution. Measurements were taken immediately after dilution.

Plots of extinction coefficient vs. Sn/Pt mole ratio at 410 nm were made to investigate the absorption behavior of the Sn-Pt complex without interference from Sn or Pt absorption at lower

wavelengths. Plots of the extinction coefficient in the UV-vis range where the Sn-Pt complex is photoactive are given in SI Figure 2. Finally, data were also collected for mixtures of Sn(IV) and Pt to determine whether Sn(IV)-Pt complexes form. The results indicate that Sn(IV) does not form UV-vis photoactive complexes.

The Sn-Pt complex will possess the stoichiometry indicated by the Sn/Pt ratio where there is a non-zero slope in plots of the extinction coefficient vs. Sn/Pt ratio. The Sn/Pt ratio data were corrected for the 1 mole of Sn reacted to reduced Pt(IV) to Pt(II). In order to apply the mole ratio method, we will plot the extinction coefficient at 410 nm vs. Sn/Pt ratio. The extinction coefficients are joined as straight line segments according to the mole ratio mathematics proposed by Meyer.<sup>1</sup> Changes in the slope of the extinction coefficient vs. Sn/Pt mole ratio indicate changes in the complex. Further spectroscopic evidence for both existence of both structures has been given previously in the literature.<sup>1-6</sup>

**SI 1.4 Color stability.** Achieving complex stability is important before taking absorbance measurements and was monitored both spectroscopically and visually. Stable deep red color of the formed Sn-Pt complexes was observed before measurements were taken. The evolution of Sn-Pt complexes was monitored using the peak appearing at approximately 410 nm over the first few minutes after mixing. The 410 nm wavelength was chosen because uncomplexed Sn and Pt are not photoactive at that wavelength thus ensuring changes in extinction coefficient are related to the complex only. Absorbance measurements were taken every two minutes for the first 20 minutes at room temperature with nitrogen bubbling. The absorbance measurements were stable after 10 minutes in the case of Pt(II) and after 15 minutes in the case of Pt(IV) and suggest that the formation of Sn-Pt complex is complete and UV-vis measurements reflect a stable complex in solution. The results of the stable measurements are given in SI Figure 2.



SI Figure 2: Molar extinction coefficient of Sn/Pt complexes formed with (a) Pt(II) and (b) Pt(IV) in 7.5 M, nitrogen-saturated hydrochloric acid. For clarity half-molar ratios were excluded from the chart except for 1.5 M and 2.5 M curves in (a) and (b), respectively. The legend is in the same order as the various curves. The following observations can be made and are important for understanding the nanoparticle growth: 1) complexes formed from Pt(II) and Pt(IV) behave identically and suggest that the Pt(IV) is reduced before forming a complex with Sn; 2) measurements taken above 400 nm are related to the complex alone without any interference from excess Sn at lower wavelengths; and 3) several of the curves overlap at 410 nm suggesting a similar complex is present as the mole ratio changes.

### SI 1.6 Determining Nanoparticle Growth Kinetics using Small Angle X-ray Scattering.

Scattering measurements were taken at the Advanced Photon Source at Argonne National Laboratory (Argonne, IL, USA) beam line 12-ID-B using monochromated 12 keV X-ray energy with two Pilatus detectors (SAXS: Pilatus2m; WAXS: Pilatus300). The beam was focused on a

0.5 mm x 1 mm window on the centerline of the quartz capillary to minimize X-ray scattering at the quartz capillary/sample interface. Scattered beam passed through vacuum to reduce absorption. The 2-dimensional SAXS flux data were azimuthally averaged and plotted versus scattering vector,  $q = (4\pi \sin \theta)/\lambda$  (in  $1/\text{\AA}$ ), where  $\theta$  and  $\lambda$  are the scattering angle and wavelength of the X-ray used, respectively. The  $q$  range spanned approximately  $0.05 \text{ nm}^{-1}$  to  $25 \text{ nm}^{-1}$ . However, features of interest were limited to the range  $0.3$  to  $10 \text{ nm}^{-1}$ .

Scattering vector,  $q$ , was calibrated using silver behenate, while scattering intensity was absolutely calibrated ( $\text{cm}^{-1}$ ) using glassy carbon.<sup>7</sup> Absolute calibration is required for determination of number density, volume fraction, and specific surface area important for kinetic analysis. Matlab R2011a (Mathworks) was used for azimuthal integration, scan averaging, and intensity scaling.  $\text{SnCl}_2$  at identical concentrations as that used in the synthesis were dissolved in 7.5 M hydrochloric acid and used as background during data analysis. IgorPro v6.2.2.2 (WaveMetrics) with the aid of the Irena<sup>8</sup> v2.42 small-angle scattering macros was used for data reduction, fitting, and modeling.

Following initial data analysis using the Irena Unified Fit tool, population distributions were modeled and fitted to the experimental data using the Modeling II package in Irena using a total non-negative least-squares algorithm. Scattering length densities determined using the scattering contrast calculator for Pt ( $145.5 \times 10^{10} \text{ cm}^{-2}$ ),  $\text{SnCl}_3$  ( $32.0 \times 10^{10} \text{ cm}^{-2}$ ), and 7.5 M HCl ( $10.2 \times 10^{10} \text{ cm}^{-2}$ ) at 12 keV. Contrast values were determined versus tin chloride dissolved in 7.5 M HCl solvent. The Sn-Pt nanoparticle scattering length density was calculated as assuming pure platinum. Populations of nanoparticles were modeled as a dilute system based on volume distributions determined using 50 points and a Gaussian distribution with a sphere form factor.<sup>9</sup> Population standard deviations,  $\sigma$ , were calculated from population FWHM according to:

$\text{FWHM}=2(2\ln 2)^{0.5}\sigma$ . These parameters gave similar mean size results to the Unified Fit tool. Scattering intensities at  $q$  larger than  $8 \text{ nm}^{-1}$  were not fitted during population modeling.

## SI 2. RESULTS AND DISCUSSION

**SI 2.1. Sn-Pt Complex EXAFS Fitting Details.** The results of the structure fitting are given in SI Table 1 while the plotted data fits are shown in SI Figure 3. SI Figure 3 demonstrates the quality of the fits, especially for the multiple scattering paths at large  $R$  and low  $k$ . The fits to the  $R$ - and  $k$ -space data in SI Figure 3 (results in SI Table 1) are for a 50:50 mix of the anions in Figure 2(b) and 2(c) of the main document. Relative material composition was determined using SI Equation 1 below

$$\frac{x_m}{x_n} = \frac{N_{R,m}}{N_{R,n}}$$

SI Eq. (1)

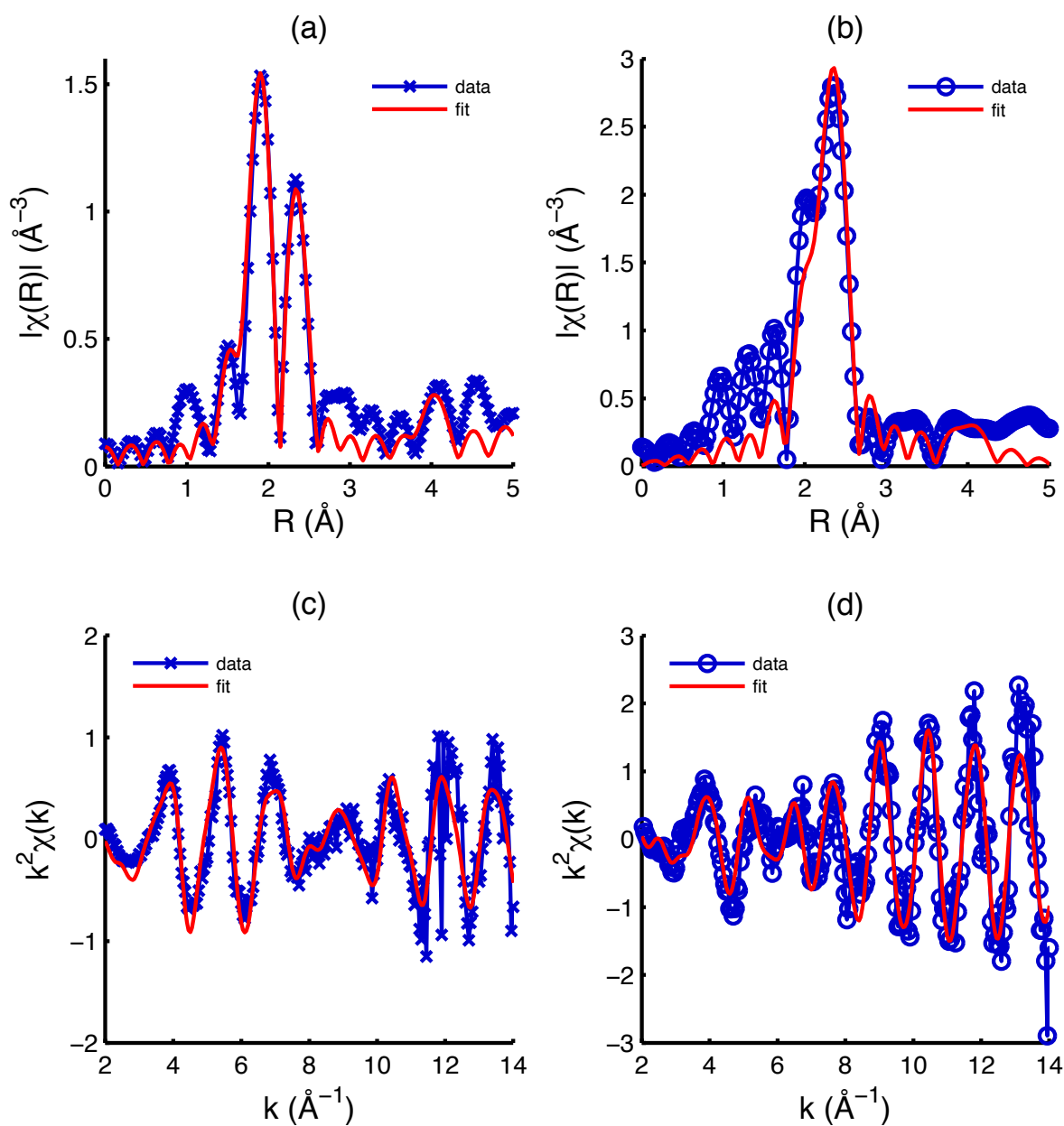
where  $x$  is the atomic fraction of elements,  $m$  and  $n$ , and  $N_R$  is the radial coordination number. The results for  $N_{R, Cl}$  and  $N_{R, Sn}$  agree with the proposed 50:50 mix of  $[\text{PtCl}_2(\text{SnCl}_3)_2]^{2-}$  and the  $[\text{PtCl}_3(\text{SnCl}_3)_1]^{2-}$  anion. The  $k^2$ -weighted  $\chi(k)$  forward FT parameters were:  $k$ -weight, 0.5; window, Hanning;  $k$ -range, 20 – 94.24  $\text{nm}^{-1}$ . The  $k^2$ -weighted  $\chi(R)$  backward FT parameters were:  $R$ -range, 0.1 – 0.6 nm; window, Hanning. Single, triangular, and multiple scattering paths were modeled for the complex to give fits at large values of  $R$ . Geometric and symmetry relationships were used to limit the number of independent parameters.

Fits were made to the EXAFS data by using atomic Cartesian coordinates for atom locations in the complex were used in FEFF<sup>10</sup> to determine scattering paths. Interference patterns were simulated and parameters were fit in Artemis.<sup>11</sup> Single, triangular, and multiple scattering paths were modeled for the complex to give fits at large values of  $R$ . This approach was important to determine the geometry of the complex. At low Sn/Pt ratios, the complex is square planar, while at higher ratios the geometry changes to accommodate higher Pt-Sn coordination. Once the first

shell oscillations were well fit, their associated Debye-Waller factors and interatomic spaces were constrained for fitting of higher shells. Once all of the Debye-Waller factors and Sn-Cl distances were determined, constraints were relaxed for the final fit.

SI Table 1: Pt L<sub>3</sub> Edge k<sup>2</sup>-Weighted EXAFS Fit Results for the [Pt(SnCl<sub>3</sub>)<sub>5</sub>]<sup>3-</sup>, the [PtCl<sub>2</sub>(SnCl<sub>3</sub>)<sub>2</sub>]<sup>2-</sup>, and the [PtCl<sub>3</sub>(SnCl<sub>3</sub>)<sub>1</sub>]<sup>2-</sup> found in Figure 2d, 2c, and 2b, respectively.

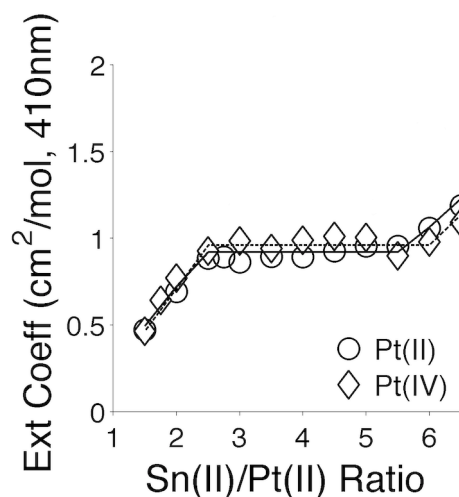
<i>model: C2/c space group [Pt(SnCl<sub>3</sub>)<sub>5</sub>]<sup>3-</sup> anion</i>				
M-M	R (nm)	ΔR (nm)	σ <sup>2</sup> (nm <sup>2</sup> )	ΔE <sub>0</sub> (eV)
Pt-Sn <sub>ax</sub>	0.2540	0.0003±0.0022	3x10 <sup>-5</sup>	4.57
Pt-Sn <sub>eq</sub>	0.2545	0.0037±0.0017	2x10 <sup>-5</sup>	4.57
Sn <sub>ax</sub> -Cl	0.2380	0.0005±0.0002	8x10 <sup>-5</sup>	4.57
Sn <sub>eq</sub> -Cl	0.2380	-0.0172±0.0207	13x10 <sup>-5</sup>	4.57
Sn <sub>ax</sub> -Sn <sub>eq</sub>	0.3595	0.0037±0.0028		
Sn <sub>eq</sub> -Sn <sub>eq</sub>	0.4408	0.0064±0.0029		
Sn <sub>ax</sub> -Sn <sub>ax</sub>	0.5080	0.0006±0.0044		
Cl-Sn <sub>ax</sub> -Pt	120°	-8°±0.1°		
Cl-Sn <sub>eq</sub> -Pt	120°	6°±8.3°		
<i>model: C1 space group [PtCl<sub>2</sub>(SnCl<sub>3</sub>)<sub>2</sub>]<sup>2-</sup> anion</i>				
<i>model: Cs space group [PtCl<sub>3</sub>(SnCl<sub>3</sub>)<sub>1</sub>]<sup>2-</sup> anion</i>				
M-M	R (nm)	ΔR (nm)	σ <sup>2</sup> (nm <sup>2</sup> )	ΔE <sub>0</sub> (eV)
Pt-Sn	0.2500	0.0005±0.0007	4x10 <sup>-5</sup>	6.93
Pt-Cl	0.2328	-0.0013±0.0008	2x10 <sup>-5</sup>	6.93
Sn-Cl	0.2391	0.0239±0.0343	3x10 <sup>-5</sup>	6.93
Cl <sub>Sn</sub> -Sn-Pt	120°	1°±5.1°		
Cl <sub>Pt</sub> -Sn-Pt	90°	0.5°±0.3°		



SI Figure 3: The Pt  $L_3$  edge ( $k^2$ -weighted) Fourier transform of the EXAFS scattering from the proposed Pt-Sn complexes. A 50:50 mix of  $[\text{PtCl}_2(\text{SnCl}_3)_2]^{2-}$  with  $[\text{PtCl}_3(\text{SnCl}_3)_1]^{2-}$  in R-space (a) and k-space (c). The  $[\text{Pt}(\text{SnCl}_3)_5]^{3-}$  anion in R-space (b) and k-space (d).

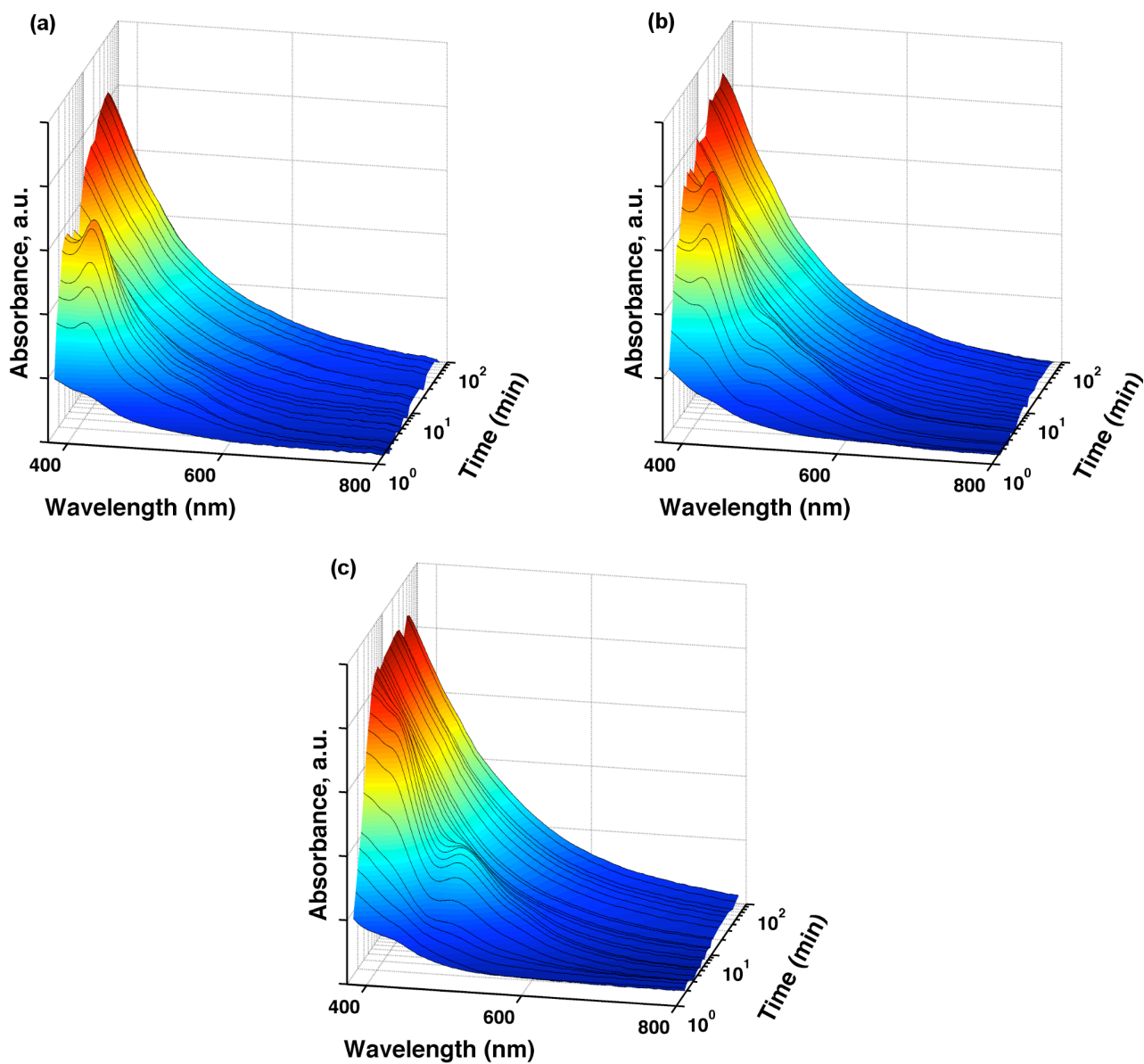
**SI 2.2. Sn-Pt Complex Stoichiometry Determination Using UV-Vis.** We used the mole ratio method to determine the atomic ratio of Sn to Pt in the complex wherein Sn-Pt complex stoichiometry. SI Figure 4 is used to show the how the extinction coefficient varies with Sn/Pt molar ratio at 410 nm, a wavelength chosen to isolate the contribution of the Sn-Pt complex from contributions related solely to Sn or Pt at lower wavelengths. The Sn/Pt mole ratio in SI Figure 4 plots Sn/Pt(II) instead of Pt(IV) because the complex forms after the reduction of Pt(IV) to Pt(II). In this way,  $\text{Sn/Pt(II)} = \text{Sn(II)/Pt(IV)} - 1$ . We will continue to refer to our Sn/Pt ratio during synthesis in terms of the raw material, Pt(IV).

The results of the mole ratio analysis suggest that for a significant portion of the mole ratio range, there is a preferred complex with a Sn/Pt(II) stoichiometry near 3, and as the Sn/Pt ratio is increased a new complex forms with a Sn/Pt(II) stoichiometry near 5. SI Figure 4 shows the behavior of molar extinction coefficient ( $\text{cm}^2/\text{mol}$ ) versus wavelength for several mole ratios. There are two slope changes that correlate with changes in the Sn/Pt(II) molar ratio in the solution. The first slope change occurs at a Sn/Pt(II) ratio of approximately 3 followed by a second slope change with a Sn/Pt(II) ratio of approximately 5. This suggests that a complex with a Sn/Pt(II) ratio of approximately 3 exists and persists as Sn/Pt(II) ratio is increased until a Sn/Pt(II) ratio of about 5 is achieved where the Sn-Pt complex changes to a 5-coordinate one. We have hypothesized structures based on our EXAFS and UV-vis data in Figure 2(b-d) and that have been previously identified in the literature.<sup>1-6</sup>



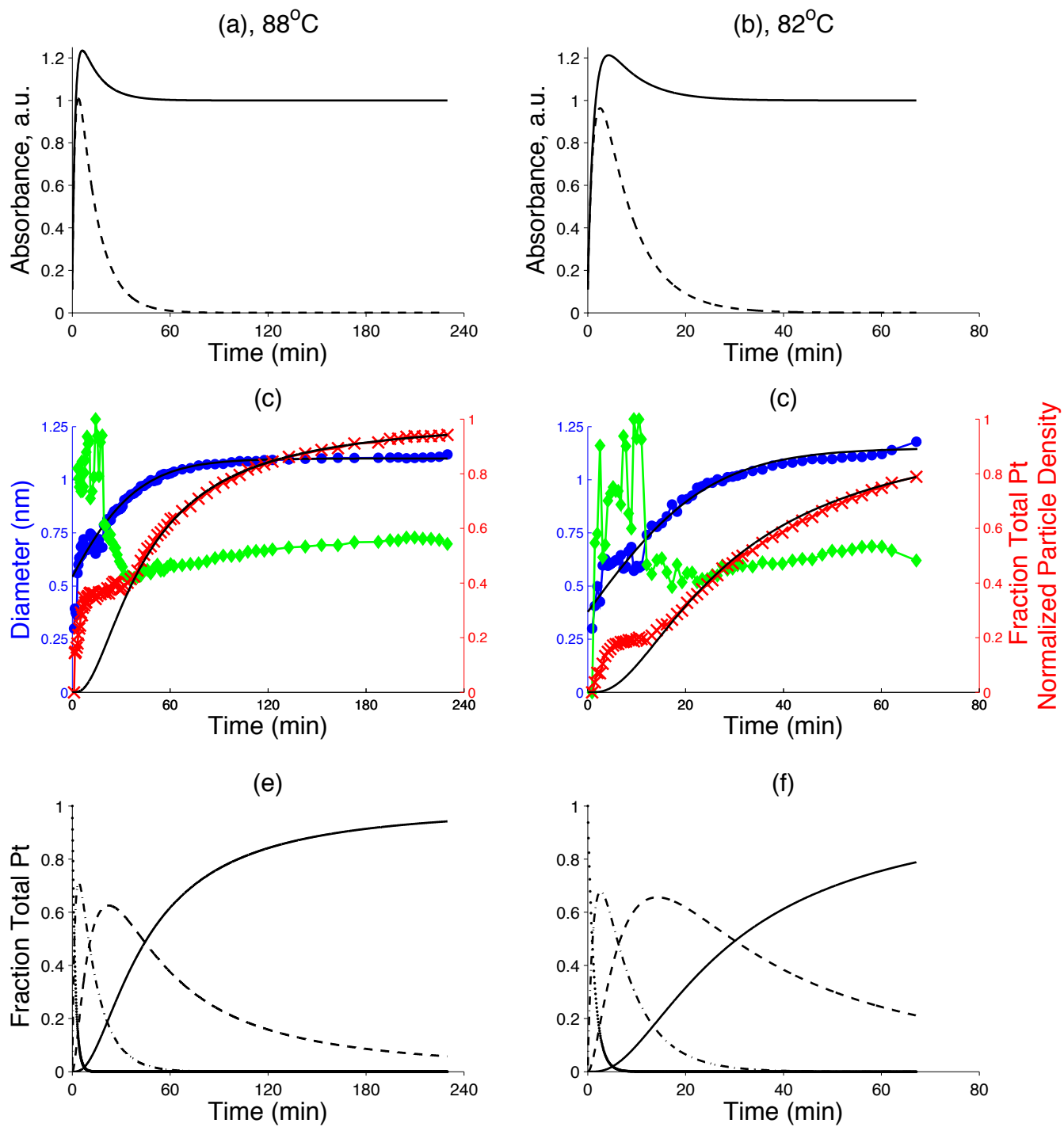
SI Figure 4: Extinction coefficient plotted versus Sn/Pt mole ratio at 410 nm. Pt(IV) data (*diamonds*). Pt(II) data (*circles*). The Sn/Pt(IV) data have been corrected for reduction to Pt(II), thus:  $\text{Sn(II)/Pt(II)} = \text{Sn(II)/Pt(IV)} - 1$ . Straight-line segments (Pt(IV) – dashed; Pt(II) – solid) indicate joined regions from the mole ratio analysis.

**SI 2.3. Sn-Pt Complex Reduction Kinetics using Time-Resolved, ex Situ UV-vis Spectroscopy.** The UV-vis absorption at 410 nm allows us to follow the progress of the Sn-Pt complex reduction by monitoring changes in concentration of the Sn-Pt complex and reduced Pt<sup>0</sup> atoms. The raw data are given in SI Figure 5 while the absorbance data at 410 nm are plotted in Figure 4(g-i) of the main document. The behavior of the peak shape at 410 nm over time is used to monitor the reduction of Pt in the Sn-Pt complex to form reduced Pt<sup>0</sup> atoms. As can be seen in SI Figure 5, the contribution from the Sn-Pt complex at 410 nm at  $t_0$  is relatively weak. As heat is applied and the temperature rises, the peak at 410 nm sharpens dramatically and then disappears rapidly as the Pt particle absorption develops as indicated in Figure 4(g-i). The appearance and disappearance of this dramatically enhanced absorption peak at 410 nm over time is attributed to complex reduction and the formation of reduced Pt<sup>0</sup> atoms. The excitation at 410 nm and electron transfer from the Sn 6p to the Pt 5d orbital has been described previously.<sup>4,5</sup>



SI Figure 5: Time-resolved, ex situ UV-vis absorption data three separate  $\text{Sn}^{2+}/\text{Pt}^{4+}$  ratios including at the reaction conditions specified in the experimental methods section: (a) 3, (b) 4, (c) 6. The appearance of a characteristic feature at 410 nm (peaks for (a) and (b), shoulder for (c)) are ascribed to the formation and consumption of a nucleated intermediate species. Absorption

greater than 600 nm is believed to be from fully reduced Pt only because of the broad absorption of Pt nanoparticles centered at 230 nm and extending deeply into the visible spectrum.



SI Figure 6: Combined SAXS/WAXS, UV-vis, and modeled data for Pt nanoparticle evolution for a  $\text{Sn}^{2+}/\text{Pt}^{4+}$  ratio of 3 at 88°C (*left column*) and 82°C (*right column*). *First row* – (a,b): Modeled UV-vis absorbance of transient peak (*dashed*) and total absorbance during growth (*solid*). Data are modeled by using rate constants obtained from temperature data generated at 60, 70, and 85°C. *Second row* – (c,d): Combined analyzed SAXS/WAXS data for primary Pt nanoparticle structure size evolution (*blue circle* – diameter, nm – left axes), fraction of total Pt (*red x* – right axes), and normalized particle density (*green diamonds* – right axes). Evolution of the equilibrium particle size is relatively slow allowing for detailed time resolution of early growth phases. Size data are fit using a modified LaMer's equation (*black line*). Volume fraction data are fit using a consecutive rate equation of arbitrary order based on the conversion of Pt primary particles into Pt nanoparticles (*black line*). *Third row* – (e,f): Fraction of total Pt for the various species consumed and produced during the course of synthesizing the Pt nanoparticles. (*dotted*) Consumption of Sn-Pt complex. (*dot-dashed*) Production and consumption of an autoreduced species. (*dashed*) Production and consumption of Pt primary particles. (*solid*) Production of Pt nanoparticle structure of the size given in (c,d). Modeled primary particle behavior peaks with experimentally determine particle density.

## REFERENCES

1. Meyer, A. S.; Ayres, G. H., The Mole Ratio Method for Spectrophotometric Determination of Complexes in Solution. *J. Am. Chem. Soc.* **1957**, *79*, 49-53.
2. Ayres, G.; Meyer, A., Spectrophotometric Study of Platinum (IV)-Tin (II) Chloride System. *Anal. Chem.* **1951**, *23*, 299-304.
3. Meyer Jr, A. S.; Ayres, G. H., The Interaction of Platinum (II) and Tin (II) Chlorides. *J. Am. Chem. Soc.* **1955**, *77*, 2671-2675.
4. Boudreaux, E. A., QR-SCMEH-MO Calculations on the Complex  $[\text{Pt}(\text{SnCl}_3)_5]^{3-}$ : Electronic Structure, UV-visible Spectrum, Magnetic Properties, and Bond Energy. *Int. J. Quantum Chem.* **2012**, *112*, 2801-2807.
5. Nelson, J. H.; Wilson, W. L.; Cary, L. W.; Alcock, N. W.; Clase, H. J.; Jas, G. S.; Ramsey-Tassin, L.; Kenney, J. W., Comparison of the Properties of  $\text{SnCl}_3^-$  and  $\text{SnBr}_3^-$  Complexes of Platinum(II). *Inorg. Chem.* **1996**, *35*, 883-892.
6. Ayres, G. H., Reactions Involving Colored Complexes of Platinum Metals. *Anal. Chem.* **1953**, *25*, 1622-1627.
7. Zhang, F.; Ilavsky, J.; Long, G. G.; Quintana, J. P. G.; Allen, A. J.; Jemian, P. R., Glassy Carbon as an Absolute Intensity Calibration Standard for Small-Angle Scattering. *Metall. Mater. Trans. A* **2010**, *41*, 1151-1158.
8. Ilavsky, J.; Jemian, P. R., Irena: Tool Suite for Modeling and Analysis of Small-Angle Scattering. *J. Appl. Crystallogr.* **2009**, *42*, 347-353.
9. Beaucage, G., Approximations Leading to a Unified Exponential/Power-Law Approach to Small-Angle Scattering. *J. Appl. Crystallogr.* **1995**, *28*, 717-728.
10. Rehr, J. J.; Kas, J. J.; Vila, F. D.; Prange, M. P.; Jorissen, K., Parameter-Free Calculations of X-Ray Spectra with FEFF9. *Phys. Chem. Chem. Phys.* **2010**, *12*, 5503-5513.
11. Ravel, B., *Crystallography for the X-Ray Absorption Spectroscopist*. University of Chicago: 2002.